HHS Public Access

Author manuscript

Bioconjug Chem. Author manuscript; available in PMC 2019 December 19.

Published in final edited form as:

Bioconjug Chem. 2019 December 18; 30(12): 3078–3086. doi:10.1021/acs.bioconjchem.9b00737.

Orientation-Controlled Bioconjugation of Antibodies to Silver Nanoparticles

Nicole E. Pollok[1], **Charlie Rabin**[1], **Leilani Smith**, **Richard M. Crooks**[*]

Department of Chemistry, The University of Texas at Austin, 100 E. 24th St., Stop A1590, Austin, TX, 78712-1224, U.S.A.

Abstract

Here we report on the use of heterobifunctional cross-linkers (HBCLs) to control the number, orientation, and activity of immunoglobulin G antibodies (Abs) conjugated to silver nanoparticles (AgNPs). A hydrazone conjugation method resulted in exclusive modification of the polysaccharide chains present on the fragment crystallizable region of the Abs, leaving the antigen-binding region accessible. Two HBCLs, each having a hydrazide terminal group, were synthesized and tested for effectiveness. The two HBCLs differed in two respects, however: (1) either a thiol or a dithiolane group was used for attachment to the AgNP; and (2) the spacer arm was either a PEG chain or an alkyl chain. Both cross-linkers immobilized 5 ± 1 Abs on the surface of each 20 nm-diameter AgNP. Electrochemical results, obtained using a half-metalloimmunoassay, proved that Abs conjugated to AgNPs *via* either of the two HBCLs were 4 times more active than those conjugated by the more common physisorption technique. This finding confirmed that the HBCLs exerted orientational control over the Abs. We also demonstrated that the AgNP-HBCL-Ab conjugates were stable and active for at least two weeks. Finally, we found that the stability of the HBCLs themselves was related to the nature of their spacer arms. Specifically, the results showed that the HBCL having the alkyl chain is chemically stable for at least 90 days, making it the preferred cross-linker for bioassays.

Graphical Abstract

[*]To whom correspondence should be addressed. crooks@cm.utexas.edu.

[1]These authors contributed equally.

Supporting Information

The Supporting information is available free of charge on the ACS Publications website at DOI:

UV-Vis spectra of 20 nm-diameter citrate-capped AuNPs before and after bioconjugation with HBCL1-modified Ab, HBCL2-modified Ab and unmodified Ab (physisorption) (Figure S1), ELISA calibration curve for determining the number of Abs per NP and histogram of the number of Abs immobilized per AuNP (Figure S2), Hydrodynamic diameter of AgNP conjugates (Table S1), Electrochemical results obtained for the off-target conjugates (Figure S3), UV-Vis absorbance results to determine the stability of NP portion of the conjugates over a 6-day period (Figure S4), ^{1}H and ^{13}C NMR spectra (400 MHz, $DMSO_{d6}$) of HBCL1 (Figure S5), ^{1}H and ^{13}C NMR spectra (400 MHz, $DMSO_{d6}$) of HBCL2 (Figure S6), Description of the electrochemical cell used for determining the activity of the Abs of the AgNP-Ab conjugates (Figure S7), COSY ($^{1}H/^{1}H$) and HSQC ($^{1}H/^{13}C$) 2D NMR spectra (400 MHz, $DMSO_{d6}$) of HBCL1 (Figure S8), COSY ($^{1}H/^{1}H$) and HSQC ($^{1}H/^{13}C$) 2D NMR spectra (400 MHz, $DMSO_{d6}$) of HBCL2 (Figure S9), Colorimetric determination of polysaccharide chains on Abs by UV-Vis using Purpald (Figure S10), AgNP and AuNP percentage yields after functionalization and centrifugation (Figure S11), Protocol for physisorption of Abs to NPs, ELISA for the comparison of activity of unmodified Ab, HBCL1-modified Ab and HBCL2-modified Ab (Figure S12), UV-Vis quantification of AgNPs and AuNPs (in particles/mL) (Figure S13), Electrochemical results obtained for the conjugates containing the same molar equivalents of Ag (without target present) (Figure S14), Electrochemical results obtained for unmodified AgNPs following 15 and 30 min of incubation with $KMnO_4$ (Figure S15), Electrochemical background of $KMnO_4$ and PBS (Figure S16).

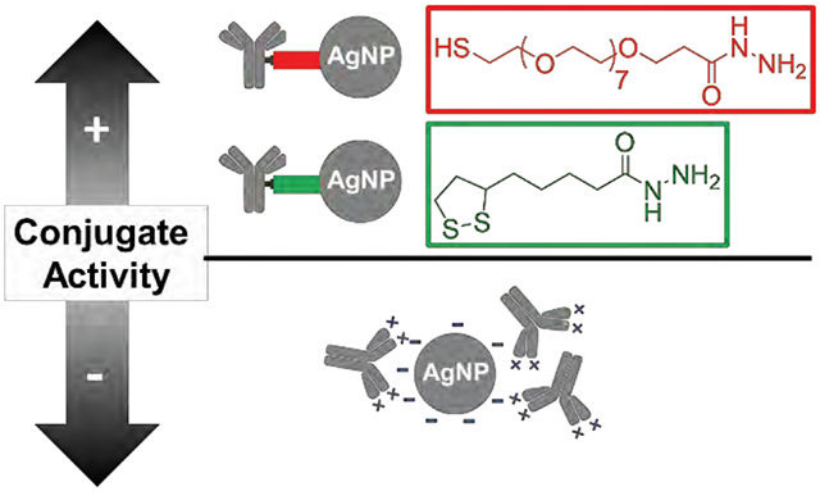

Introduction

In this paper we demonstrate the use of heterobifunctional cross-linkers (HBCLs) to control the number and orientation of immunoglobulin G antibodies (Abs) conjugated to silver nanoparticles (AgNPs). Specifically, two HBCLs were synthesized, each bearing: (1) a hydrazide group for the specific targeting of the fragment crystallizable (Fc) region of Abs,[1–4] (2) a thiol group for anchoring the HBCL to the AgNP,[3,5–8] and (3) a tunable spacer arm to enhance the biocompatibility[1] of the NP-Ab conjugates. The key finding is that HBCLs improve the activity of the Abs on AgNPs by helping to control their orientation compared to the more common physisorption method in which Abs can be randomly arranged electrostatically.[1,9] Because AgNPs have become increasingly important as labels for bioassays[10,11] in recent years, and because there are few prior reports relating to controlled-Ab immobilization on AgNPs,[9,13] the present study is timely and relevant.

While Au and Ag are both noble metals, Au has a significantly higher standard potential (E^0 = 1.52 V) than Ag (E^0 = 0.79 V).[14] The increased stability of AuNPs relative to AgNPs makes them a prime candidate for bioconjugation applications. Indeed, there are numerous reports of Ab immobilization on AuNPs.[3,12,15,16] In recent years, however, AgNPs have been shown to have optical[10,11,17,18] and biological[17,19,20] properties that can be beneficial to the development of a new category of molecular probes. For example, our group has used AgNPs as a signal amplifying label for detecting Abs in metalloimmunoassays,[21–23] including for electrochemical detection of the heart-failure biomarker, N-terminal prohormone brain natriuretic peptide (NT-proBNP).[24] In this specific metalloimmunoassay, simple physisorption was used to conjugate the detection Abs to the AgNP labels. The detection limit and reproducibility of this approach were not satisfactory, however, and therefore we sought an alternative immobilization method.

Physisorption of Abs to metal NPs relies primarily on interactions between the NP surface and amine or thiol residues present on the Abs.[1,25] While this approach for bioconjugation is fast and easy, it has four important limitations: (1) it requires a large excess of Abs which can lead to surface crowding;[1,2,20] (2) the Ab coverage on the NP surface is not well-

controlled;[1] (3) the stability of the conjugate is poor due to weak electrostatic interactions;[12,26,27] and (4) the lack of control over the orientation of the Abs reduces access of the target to the antigen-binding sites (Fab).[1,12]

Recent results reported by Siriwardana and coworkers have demonstrated that the foregoing shortcomings can, to a significant degree, be avoided by genetically engineering the Fc region of Abs.[28] For example, Driskell and coworkers showed that the stability and orientation of anti-horseradish peroxidase Abs on AuNPs could be improved by controlling the charge distribution of the Abs.[15] They also showed that the interaction between these Abs and AuNPs is irreversible and that the physisorbed Abs resist displacement by plasma proteins.[29] While these results provide a promising route to controlling the structure of physisorbed abs, the use of HBCLs comprised of a thiol group at one end and a Fc region-conjugated Ab on the other is far more common and in most cases highly effective. Like Au,[4,30,31] Ag can also form dative bonds with thiol functional groups,[5–8,32–36] which provides a means for forming a stable bond between the Ag surface and the Fc region of the Abs.

As mentioned earlier, the majority of reports pertaining to Ab immobilization on AgNPs do not rely on a controlled immobilization method. For example, in 2007 Huang *et al.* used the affinity of thiols for AgNPs to link Abs to AgNPs *via* an HBCL.[37] Specifically, they attached thiolated HBCLs to the surface of AgNPs, and then activated the carboxylic acid group at the distal end of the HBCLs using 1-ethyl-3-(3-dimethylaminopropyl)carbodiimide. Exposure of these functionalized AgNPs to Abs resulted in a reaction between the activated carboxylic acids of the HBCL and primary amines present on the Abs.[38] A related approach has also been reported in which activated carboxylic acids present on the Abs were reacted with thiol/amine HBCLs pre-attached to AgNPs.[2]

Both of the foregoing approaches rely on the position of accessible amine or carboxylic acid groups within the Ab structure, which is strongly dependent of the Ab sequence. The main drawback of targeting amine and carboxylic acid groups is, therefore, the lack of control over the distribution of the functional groups on the Ab. Indeed, charged residues (NH_3^+ and COO^-) are randomly distributed in the Ab amino acid sequence. Moreover, targeting amine groups has an even more deleterious effect upon binding activity of Abs because the N-terminus is located within the Fab region.[1,9,39–42] This potentially puts the active site of the Ab in danger of being damaged or misoriented on the surface of the NPs. In these cases, like in the physisorption method, control over the orientation is not achieved.

To overcome some of the deficiencies of these earlier approaches, we focused on controlling the orientation of the Abs to allow the Fab regions to be more accessible to antigens in solution while still maintaining a robust AgNP-Ab interaction.[43] This can be done by targeting either the C-terminus of the Ab or the polysaccharide chains sequestered in the Fc region.[1,2,44] The C-terminus is generally recognized by specific protein/protein interactions with protein G[9,13] or protein A,[12] but in both cases this is a reversible binding event.[9,45] In contrast, the polysaccharide chains can either be targeted directly with boronic acid residues,[2,46,47] or by following a mild oxidation step coupled with a hydrazide addition.[1,40] Because the boronic-polysaccharide complex is known to be unstable at physiological pH,[47] we elected to use the hydrazone chemistry. Scheme 1 depicts the hydrazone method, in which

the polysaccharide chains of the Ab are first converted to aldehyde groups with a mild oxidant, and then coupled to hydrazide-functionalized HBCLs. Note that a similar approach was reported by Kumar *et al.* in 2008 for AuNPs, and as we will show later AgNPs are as biocompatible as AuNPs using this approach.[3]

In the present article, two HBCLs differing in spacer arm composition (PEG or alkyl chains) and sulfur group (thiol or dithiolane) were synthesized and used to conjugate Abs to 20 nm AgNPs (Scheme 1). 27-(1-mercaptononyl)-3,6,9,12,15,18,21,24-octaoxaheptacosanoyl-hydrazide and (1,2-dithiolan-3-yl)pentanoyl-hydrazide will be referred to as HBCL1 and HBCL2, respectively. The same chemistry was carried out using AuNPs as a benchmark for comparison. The present study shows that: (1) a HBCL-mediated bioconjugation method can be used to efficiently functionalize AgNPs; (2) NPs can be functionalized with reproducible numbers of Abs; (3) HBCLs lead to Ab orientation on NP surfaces that results in improved binding of targets compared to physisorption; and (4) the binding efficiency to the target is constant over at least a two week period for AgNP-HBCL-Ab conjugates, which is not the case for physisorbed conjugates.

Results and Discussion

Characterization of the AgNP-Ab conjugates.

The hydrazone bioconjugation method has been used previously for preparing AuNP-Ab conjugates,[3] but to the best of our knowledge there are no such reports of HBCL-modified Abs being conjugated to AgNPs. The main goal of the present article, therefore, is to show that hydrazone bioconjugation is possible with AgNPs and that it is a superior alternative to physisorption. To accomplish this, AgNPs were conjugated with Ab-HBCL1, Ab-HBCL2, and unmodified Abs (physisorption), and resulting materials were characterized.

Figure 1 shows representative UV-Vis spectra for unconjugated 20 nm AgNPs and the three Ab conjugates. The characteristic plasmon band for the unmodified, citrate-capped AgNPs is present at λ_{max} = 395 nm (black trace). After functionalization with Ab-HBCLs or unmodified Abs, the plasmon band undergoes a red-shift of 3 nm (red and green traces) and 5 nm (blue trace), respectively. This red shift is in agreement with a change in the refractive index of the environment surrounding the metallic NPs,[48,49] which is characteristic of bioconjugation. Note that the spectra depicted in Figure 1 are normalized to a λ_{max} intensity of 1.0 to better highlight the red shift. The same experiments were carried out with AuNPs as a benchmark, and the results are shown in Figure S1. In this case a similar red shift of 3 to 5 nm was observed. From these results, we conclude that the AgNPs have been successfully conjugated to the Abs. In a subsequent section we will discuss the extent of conjugation.

Quantification of the total number of Abs per AgNP.

It is usually not possible to directly quantify the number of Abs or proteins on a solid phase, such as a NP, because the solid phase can interfere with the analysis.[1] To avoid such interferences, destructive techniques can be used. These include dissolution of the metal NP to prevent fluorescence quenching,[50–52,53,54] or complete digestion of the conjugate followed by high-performance liquid chromatography to determine the total protein content

on the NP.[55] However, we wanted to avoid destructive techniques so that it would be possible to compare every batch of conjugates without having to sacrifice samples. Thus, an indirect quantification method was used; that is, measuring the amount of unbound Abs remaining after bioconjugation.

The number of unbound Abs for the three conjugates in this study were determined as follows. First, the conjugation reaction was carried out. Second, the supernatant resulting from the first centrifugation (washing) step, which contains the unbound Abs, was collected. Third, an indirect ELISA was performed following the procedure described in the Experimental Section.

Figure 2 is a histogram of the results from the indirect ELISA. The data represent results obtained from three independent reactions for each conjugate. Interestingly, the coverage is strongly dependent on the conjugation method. More specifically, using the hydrazone chemistry, 5 ± 1 Abs are reproducibly immobilized per AgNP for both HBCLs, while approximately three times more Abs are directly physisorbed to the AgNPs. These trends are similar to those we determined for AuNPs (Figure S2).

To ensure that the foregoing results are within a reasonable range, we calculated the approximate maximum Ab coverages for our materials. By considering typical dimensions for an Ab (14.5 nm × 8.5 nm × 4 nm),[39] the surface area of a smooth 20.0 nm-diameter sphere (1260 nm^2), and the orientation of the surface-confined Abs, it is possible to estimate maximum coverage. Using this approach, the maximum coverage for Abs oriented side-on is 10, while for end-on coverage it is 40. As shown in Figure 2, the coverage of physisorbed Abs on 20 nm AgNPs is 15 ± 2 Abs/NP, which is almost the same as we measured for physisorption onto AuNPs (13 ± 2 Abs/NP, Figure S2). This suggests that, independent of the metal, physisorbed Abs are present in both side-on and end-on orientations. There may also be Ab-Ab interactions that result in bilayer formation.

In contrast to physisorption, Abs immobilized *via* the hydrazone method should bind only in an end-on orientation due to the positioning of the HBCLs on the Fc region of the Ab. This configuration should result in higher activity. Evidence for significant structural differences between physisorbed Abs and those linked *via* the HBCLs comes from dynamic light scattering measurements. The increase in hydrodynamic diameter (Δ_H) of the physisorbed materials was found to be 24.6 ± 1.2 nm, while for the materials having HBCLs the Δ_H were 9.4 ± 0.7 and 7.1 ± 1.3 nm for AgNP-HBCL1-Ab and AgNP-HBCL2-Ab, respectively.

Comparison of the Ab activity of the conjugates.

To confirm the orientations of the Abs, our next step was to quantitatively compare their binding activity for a specific antigen, NT-proBNP. The basis for correlating antigen-binding activity to orientation is the well-known fact that only an accessible and intact Fab region will bind its antigen.[1,12] Here, Ab activity was directly determined using the half-metalloimmunoassay described in the Experimental Section. Briefly, the target, NT-proBNP, was adsorbed to the wells of a microtiter plate, then the AgNP-labeled Ab conjugates were introduced, and after washing, the amount of Ag present in each well was determined by anodic stripping voltammetry (ASV). In this assay, only the active fraction of the Abs will

bind to the immobilized target, and therefore the amount of Ag charge collected is indicative of Abs having an end-on (active) orientation.[39]

Figure 3 shows Ag ASV traces for the half-metalloimmunoassay formed with the AgNP-Ab conjugates. Each trace is representative of three individually formed half-metalloimmunoassays that were tested on three independently prepared electrodes. The blank for this experiment consisted of citrate-capped AgNPs suspended in SBB with no Abs present. Both AgNP-HBCL-Ab conjugates (red and green traces) yielded an average Ag charge of 1.68 ± 0.20 μC, while the physisorbed conjugate (blue trace) gave just 0.41 ± 0.06 μC. It should be noted that an additional control experiment was performed with an off-target Ab to ensure that the HBCL itself does not play a role in binding of the Ab to NT-proBNP immobilized on the plate (Figure S3).

This experiment clearly proves the superiority of the hydrazone conjugation method compared to the more common physisorption technique. Specifically, despite a lower quantity of immobilized Abs (5 vs. 15 for the HBCL and physisorbed conjugates, respectively), the higher charge obtained for the AgNP-HBCL-Ab conjugates is evidence of Abs being in a more active orientation. On the other hand, the lower charge resulting from the physisorbed conjugates can be related to misorientation of the Abs on the AgNP surface. Additionally, the weak electrostatic interactions might not have been sufficient to keep the Abs on the AgNP surface during formation of the metalloimmunoassay. The key point is that HBCLs help to circumvent these drawbacks.

Determination of the stability of the Abs.

To more fully characterize the AgNP-HBCL-Ab conjugates, their stability (Figure S4) and that of the Abs on the AgNP were examined. The stability of the Ab portion of the conjugates was determined electrochemically using the protocol described in the previous section. The only difference being that the assay was carried out on 0, 1, 2, 6, and 14 days after the conjugates were prepared. Day 0 corresponds to the day they were first assembled.

Figure 4 is a plot of the Ag charge resulting from the ASV analysis of the half-metalloimmunoassays as a function of time. The AgNP-HBCL1-Ab and AgNP-HBCL2-Ab conjugates, shown in red and green respectively, display the same average activity throughout the 14-day study. This is an important result, because typically the stability of metal-conjugated Abs is not reported (only the stability of the NPs is reported). The outcome of this stability study is beneficial for many applications, because it is important to know how reliable the NP-Ab conjugates are in solution for a given amount of time. In contrast to the HBCL conjugates, the physisorbed conjugates (blue) underwent a nearly 60% decrease in activity between day 0 and day 1. This decrease from 0.41 ± 0.06 μC to 0.17 ± 0.02 μC is in accord with the poor stability of other physisorbed conjugates reported in the literature.[12,26,27] Specifically, the electrostatic interactions between Abs and NPs are weak and lead to desorption over time.[1] Additionally, it is well-known that protein-surface interactions may induce conformational changes in Abs after some time. This is due to the physisorbed Abs slowly reconfiguring their packing to reach equilibrium. This process may also cause the protein to unfold and lose activity.[56]

Investigation of the stability of the HBCLs.

This part of our study focused on the relative stability of the two HBCLs. The preceding results have demonstrated that despite differences in their chemical compositions, HBCL1 and HBCL2 are equivalent in terms of conjugation efficiency and Ab stability. On the other hand, assays performed with HBCL1 tended to produce irreproducible results over a time period of a few months (data not shown). Such a decrease in bioconjugation efficiency can potentially be caused by a time-dependent change at either end (thiol or hydrazide) of the cross-linker resulting in poor attachment of the HBCL to the NP or the Ab, respectively. Thus, an NMR stability study was performed on HBCL1 and HBCL2 to identify possible structural changes. Note: this part of the study was focused on just the cross-linkers, not the conjugates.

Figure 5 presents the ^{1}H and ^{13}C NMR spectra and chemical shifts for the methylene group closest to the hydrazide-end of HBCL1, marked as (*), resulting from a 90-day study. In Figure 5a and 5b, the NMR spectra of HBCL1 is shown for days 0 and 90, respectively. Figure 5c presents the spectra of SH-PEG_7-COOH, a possible degradation product of HBCL1. After 90 days, the protons of the methylene group (*) underwent a strong deshielding from 2.34 to 2.42 ppm, meanwhile the carbon underwent a slight shielding from 67.3 to 66.4 ppm. This means that the composition of the adjacent carbo-hydrazide group was altered. The chemical shifts obtained at day 90 correspond perfectly to the signature shifts of SH-PEG_7-COOH. The correlation of the NMR shifts confirms the transformation of HBCL1 into a non-reactive form.

Finally, no evidence of chemical shifts was observed for HBCL2 over the 90-day test duration, which confirms that HBCL2 is chemically stable within this time frame in aqueous solution (Figure S6). We attribute the increased stability to the difference in the composition of the spacer arms (PEG vs. alkyl chains). Presumably, the PEG residues affect the solubility of the molecule and bring a water-rich environment close to the hydrazide, while the alkyl chain will have the opposite effect. All in all, these findings show that HBCL2 is the more advantageous cross-linker, and therefore it is the better choice for bioassays.

Summary and Conclusions

To summarize, the goal of this study was to develop a nearly universal route for conjugating Abs to AgNPs. We elected the hydrazone bioconjugation method, because it provides control over the orientation of the Abs by targeting the Fc region of Abs. We also took advantage of the affinity of the thiol endgroup for the AgNP surface. Using this generalized format, two novel HBCLs were synthesized with each bearing a hydrazide group for forming the hydrazone bond with the Abs, and a thiol group for forming a dative bond with the AgNP surface. The results showed that the AgNP-HBCL-Ab conjugates are reproducible and consist of an average of 5 ± 1 Abs per AgNP.

Using a half-metalloimmunoassay, it was possible to show that the hydrazone bioconjugation method significantly improves the activity of the conjugated Abs compared to the more common physisorption technique. Moreover, the AgNP-HBCL-Ab conjugates are stable for at least 14 days, while the physisorbed conjugates exhibit a sharp decrease in

stability one day after preparation. Finally, we found that the spacer arm of the HBCLs plays an important role in the stability of the hydrazide group of the cross-linker. More specifically, an alkyl chain spacer confers significantly more stability to the HBCL than a PEG spacer.

In conclusion, the method reported here provides a viable route for conjugation of AgNPs to Abs. This finding is significant given the recent interest in using AgNPs as electrochemical[21–23] and spectroscopic[10,11,17,18] labels for bioassays. Indeed, we are currently using the AgNP-HBCL2-Ab conjugate as a key component of a point-of-care electrochemical sensor for heart failure.[24] The results of that work will be reported in due course.

Experimental Procedures

Chemicals and materials.

All solutions were prepared using deionized (DI) water (>18.0 MΩ-cm, Milli-Q Gradient System, Millipore, Burlington, MA). Tetrahydrofuran (THF) anhydrous, hydrazine monohydrate, hydrazine solution 1 M in THF, (±)-α-lipoic acid, methanol, dimethyl sulfoxide (DMSO) and DMSO-d_6 were purchased from Sigma-Aldrich (Milwaukee, WI). 4-Amino-3-hydrazino-5-mercapto-1,2,4-triazole (Purpald), H_2SO_4, $KMnO_4$, toluene, phosphate buffered saline (PBS) pH 7.4 (P3813), casein, superblock blocking buffer (SBB) (37515), siliconized low-retention microcentrifuge tubes, Whatman grade 1 chromatography paper (180 μm thick, 20 cm × 20 cm sheets, linear flow rate of water = 0.43 cm/min), and Costar 3590 high-binding microtiter plates were purchased from Fisher Scientific (Pittsburgh, PA).

All PBS used was 1× concentration PBS. SH-PEG_7-COOH was obtained from Polypure (Oslo, Norway). mPEG-SH 5 kDa was obtained from Nanocs (New York, NY). 1-Step Ultra TMB-ELISA Substrate Solution (34028) and sodium meta-periodate ($NaIO_4$) were obtained from Thermo Scientific (Grand Island, NY). Citrate-capped AgNPs and AuNPs (nominal 20 nm diameter) were purchased from nanoComposix (San Diego, CA). N-terminal prohormone brain natriuretic peptide (NT-proBNP) and monoclonal immunoglobulin G anti-NT-proBNP 13G12 (Ab) were obtained from HyTest (Turku, Finland). Polyclonal anti-mouse immunoglobulin G horseradish peroxidase-labeled secondary antibody (SAb) was obtained from Abcam (Cambridge, UK). Amicon ultra 0.5 mL centrifugal filters (10 K) were purchased from Millipore Sigma (Tauton, MA). Conductive carbon paste (Cl-2042) was purchased from Engineered Conductive Materials (Delaware, OH). All chemicals and reagents were used without further purification unless otherwise specified.

Instrumentation.

^1H and ^{13}C NMR spectra were recorded with a Varian MR 400 MHz spectrometer while 2D NMR spectra (COSY $^1H/^1H$ and HSQC $^1H/^{13}C$) were recorded with an Agilent MR 400 MHz spectrometer. All spectra were measured using $DMSO_{d6}$ as the solvent. Multiplicities are reported as follows: s=singlet, t=triplet, m=multiplet. Chemical shifts are reported in δ

units to 0.01 ppm precision for ^{1}H and 0.1 ppm for ^{13}C by using residual solvent as an internal reference.

Absorbance measurements were obtained and pathlength corrected using a Synergy H4 Hybrid Multi-Mode Microplate Reader from BioTek (Winooshi, VT). A Sorvall Legend Micro 21R Centrifuge from Thermo Scientific was used for washing and separation steps during bioconjugation. A Mini Vortexer 945300 from VWR International (Radnor, PA) was used to briefly mix solutions while a BioShake iQ from Quantifoil Instruments GmbH (Jena, Germany) was used for incubation steps during bioconjugation. Before analysis with the microplate reader, a centrifuge 5810 R from Eppendorf (Hamburg, Germany) was used to remove bubbles from the wells.

Electrochemistry.

All electrochemical measurements were performed using a CH Instruments model 760B electrochemical workstation (Austin, TX), and a slightly modified, previously published protocol.[32] Specifically, all electrochemical materials, the working, counter, and quasi-reference electrodes were fabricated by stencil-printing carbon paste onto wax-patterned sheets of chromatography paper that had been printed using a Xerox ColorQube 8570DN printer. Following printing, the wax was melted through the thickness of the paper by placing it in an oven at 120 °C for 25.0 s. Photopaper was glued to the back of the wax printed chromatography paper for rigidity, and then it was cut into 12 rectangles (2.0 cm × 5.0 cm). A stencil for defining the 3.0 mm-diameter disk-shaped working electrode, hook-shaped carbon quasi-reference electrode, and counter electrode was created using CorelDRAW (Ottawa, ON). The stencil was cut into a thin plastic sheet of transparency film using an Epilog laser engraving system (Zing 16). Finally, the stencil was placed over the paper (wax side up), the electrodes were printed through the stencil using conductive carbon paste, and then the carbon paste was left to dry in air for 14 h (Figure S7).

Synthesis of HBCL1.

To a solution of SH-PEG_7-COOH (108 mg, 0.24 mmol) in methanol (2.00 mL) was slowly added a solution of hydrazine hydrate (1.40 mL) in methanol (1.00 mL). The reaction medium was stirred for 24 h at room temperature (RT) (22 ± 3 °C). The solvent was then co-evaporated with toluene under reduced pressure to yield HBCL1 as a yellowish oil (113 mg, 100%). ^{1}H NMR (400 MHz, $DMSO_{d6}$), δ (ppm): 3.64 (t, J = 6.5 Hz, 2H, **Hb**), 3.57 (t, J = 6.7 Hz, 2H, **Hd**), 3.51 (s, 28H, **Hc**), 2.89 (t, J = 6.4 Hz, 2H, **Ha**), 2.34 (t, J = 6.7 Hz, 2H, **He**). ^{13}C NMR (400 MHz, $DMSO_{d6}$), δ (ppm): 173.7 (C_q, **Ch**), 69.8 (CH_2, **Cd**), 69.6 (CH_2, **Ce**), 69.5 (CH_2, **Cc**), 68.6 (CH_2, **Cb**), 67.3 (CH_2, **Cf**), 37.9 (CH_2, **Ca**), 36.3 (CH_2, **Cg**). 2D NMR: COSY ($^{1}H/^{1}H$), HSQC ($^{1}H/^{13}C$). NMR spectra can be found in the Supporting Information (Figures S5 and S8).

Synthesis of HBCL2.

To a solution of (±)-α-lipoic acid (50 mg, 0.24 mmol) in anhydrous THF (3.00 mL) at 0 °C was slowly added a solution of hydrazine hydrate in THF (0.34 mL, 1 M). The reaction medium was stirred for 90 min at 0 °C. The solvent was then evaporated under reduced pressure below 30 °C to yield HBCL2 as a white solid (40 mg, 76%). ^{1}H NMR (400 MHz,

$DMSO_{d6}$), δ (ppm): 3.59 (hidden, determined by 2D NMR) (m, 2H, **Hc**), 3.12 (m, 2H, **Ha**), 2.40 (m, 1H, **Hb**), 2.10 (t, *J* = 7.1 Hz, 2H, **Hg**), 1.86 (m, 1H, **Hb'**), 1.65 (m, 1H, **Hd**), 1.52 (m, 1H, **Hd'**), 1.48 (m, 2H, **Hf**), 1.35 (m, 2H, **He**). ^{13}C NMR (400 MHz, $DMSO_{d6}$), δ (ppm): 175.2 (C_q, **Ch**), 56.5 (CH, **Cc**), 40.1 (hidden, determined by 2D NMR) (CH_2, **Cb**), 38.5 (CH_2, **Ca**), 34.4 (CH_2, **Cg**), 34.1 (CH_2, **Cd**), 28.6 (CH_2, **Ce**), 24.7 (CH_2, **Cf**). 2D NMR: COSY ($^1H/^1H$), HSQC ($^1H/^{13}C$). NMR spectra can be found in the Supporting Information (Figures S6 and S9).

Conjugating Abs to NPs.

Unless stated otherwise, all incubation steps were performed at RT at 600 rpm. To start, 5.0 μL of 6.7 μM Ab were incubated with 5.0 μL of 50 mM $NaIO_4$ for 30 min in the dark to oxidize the polysaccharide chains on the Fc region of the Ab (Figure S10). The oxidation reaction was quenched with 125 μL of PBS. The oxidized Abs were then incubated with 5.0 μL of 5.0 mM of the desired HBCL solution for 2 h. HBCL1 was directly dissolved in DI water to give the desired concentration, while HBCL2 was first dissolved in DMSO and then diluted in DI water. The solution was transferred to an Amicon ultra 0.5 mL centrifugal filter (10 K) and was centrifuged for 25 min at 4 °C at 14,000 g.

The HBCL-modified Abs were then incubated with 500 μL of the desired NP solution (4.9×10^{11} AgNPs/mL or 7.4×10^{11} AuNPs/mL) for 1 h. In this step, the microcentrifuge tubes were pre-blocked with SBB to prevent non-specific binding of Abs and NPs on the walls of the tubes. These tubes were covered with aluminum foil to protect the NPs from light. Following incubation, 50 μL of 10.0 μM mPEG-SH were added and incubated for another 20 min. Finally, three centrifugation (25 min, 4 °C, 16,600 g) steps were performed to remove unbound material, followed by resuspension into 500 μL SBB. The percentage yields of NPs after functionalization can be found in Figure S11. Henceforth, the product of bioconjugation will be referred to as NP-HBCL-Ab conjugates (AgNP-HBCL-Ab when referring to Ag and AuNP-HBCL-Ab when referring to Au). The protocol for making the samples with physisorbed Abs can be found in the Supporting Information.

Quantifying the total number of Abs per NP.

The number of Abs per NP was determined using an indirect enzyme-linked immunosorbent assay (ELISA) with a SAb. Unless stated otherwise, all incubation steps were performed for 30 min at RT at 600 rpm and were followed by three washing steps with PBS. Briefly, 100 μL of 58.2 nM NT-proBNP in PBS were incubated for 14 h at 4 °C without shaking in a high-binding microtiter plate. Then, 400 μL of 2% (w/v) casein solution in PBS were added to block the wells for 30 min without shaking. Wells used for the calibration curve (Figure S2) were incubated with various known concentrations of unmodified Abs, while test wells were incubated with the supernatant obtained after the first centrifugation (containing unbound Abs). Unmodified Abs were used for this calibration curve because ELISA results demonstrated that the conjugation process did not affect the activity of the Abs (Figure S12).

Next, 100 μL of 6.7 μM SAb were added to each well and incubated. Finally, 100 μL of the 1-Step Ultra TMB solution were added and 50.0 μL of 2 M H_2SO_4 were used to quench the reaction after it reached the desired color intensity (~3 min). The number of Abs in the

conjugates was obtained by subtracting the Ab content remaining in the supernatant after bioconjugation from the initial Ab solution. This value was divided by the number of NPs, which was determined with a calibration curve that can be found in the Supporting Information (Figure S13).

Monitoring the Ab activity of the conjugates.

The activity of the Abs on the AgNPs was determined electrochemically by forming a half-metalloimmunoassay, wherein the AgNPs were used as the detection label and the target was bound to a well. Unless stated otherwise, all steps were performed at RT at 600 rpm. Briefly, 100 μL of 0.60 μM of NT-proBNP were bound to the wells of a high-binding microtiter plate for 14 h at 4 °C. It should be noted that the NT-proBNP was immobilized in a two orders of magnitude concentration excess compared to the maximum amount of unbound Abs in these experiments (HBCL-modified Abs for AgNP-HBCL-Ab conjugates and unmodified Abs for the physisorbed conjugates). After coating the wells, the plate was washed three times with PBS and blocked with SBB for 30 min without shaking. Next, 100 μL of the conjugates were added to each well, incubated for 30 min, and washed with PBS.

To prepare for electrochemical analysis, 46 μL of PBS and 30 μL of 0.2 mM $KMnO_4$ were added to the wells to denature the metalloimmunoassay and oxidize all bound AgNPs (Figure S14). After 15 min (a sufficient amount of time) of incubation at 1000 rpm, the entire content of the well (in a single drop) was then placed on an electrode for electrochemical analysis (Figure S15). Next, the working electrode was stepped from 0 to −0.70 V vs. a carbon quasi-reference for 800.0 s to electrodeposit Ag^+ in solution to Ag^0 on the electrode surface. After electrodeposition, anodic stripping voltammetry (ASV) was used to determine the Ag content on the working electrode surface. ASV was carried out by sweeping the working electrode potential from −0.70 to 0.20 V at 50 mV/s to oxidize Ag^0. The ASV traces were background subtracted (Figure S16). The charge under the voltammogram was then determined by integration. It is important to note that this experiment was not intended to quantify total Ag from the assay since it relied solely on the diffusion of Ag^+ to the electrode surface, nonetheless, a variation in the Ag charge was obtained for the three conjugates.[14] This analysis was completed for identically prepared conjugate samples on days 0, 1, 2, 6, and 14, where day 0 represents the day the AgNPs were first conjugated to Ab-HBCL1, Ab-HBCL2, and unmodified Abs. The Ag content was then correlated to the Ab activity of the conjugates. The stability of the AgNP portion of the conjugates was also tested using UV-Vis spectroscopy, and these results can be found in the Supporting Information (Figure S4).

Supplementary Material

Refer to Web version on PubMed Central for supplementary material.

Acknowledgments

Research reported in this publication was supported by the National Heart, Lung, and Blood Institute of the National Institutes of Health under Award R01HL137601. The content is solely the responsibility of the authors and does not necessarily represent the official views of the National Institutes of Health. We also thank the Robert A. Welch Foundation (Grant F-0032) for sustained support of our research. We acknowledge Mr. Logan Wilder (UT

Austin) for helping in DLS measurements. We acknowledge Dr. Charuksha Walgama (UT Austin) for providing the electrochemical cell set-up. We also gratefully acknowledge many fruitful discussions with Dr. Ian Richards (Interactives Executive Excellence, LLC).

References

(1). Hermanson GT (2013) Bioconjugate Techniques; (Audet J, Preap M, Eds.); Academic Press.

(2). Sivaram AJ, Wardiana A, Howard CB, Mahler SM, and Thurecht KJ (2018) Recent Advances in the Generation of Antibody–Nanomaterial Conjugates. Adv. Healthc. Mater 7, 1–25.

(3). Kumar S, Aaron J, and Sokolov K (2008) Directional Conjugation of Antibodies to Nanoparticles for Synthesis of Multiplexed Optical Contrast Agents with Both Delivery and Targeting Moieties. Nat. Protoc 3, 314–320. [PubMed: 18274533]

(4). Joshi PP, Yoon SJ, Hardin WG, Emelianov S, and Sokolov KV (2013) Conjugation of Antibodies to Gold Nanorods through Fc Portion: Synthesis and Molecular Specific Imaging. Bioconjugate Chem 24, 878–888.

(5). Love JC, Estroff LA, Kriebel JK, Nuzzo RG, and Whitesides GM (2005) Self-Assembled Monolayers of Thiolates on Metals as a Form of Nanotechnology. Chem. Rev 105, 1103–1169. [PubMed: 15826011]

(6). Porcaro F, Marini C, Venditti I, Fratoddi I, Carlini L, Simonelli L, Olszewski W, Meneghini C, Luisetto I, Battocchio C, et al. (2016) Synthesis and Structural Characterization of Silver Nanoparticles Stabilized with 3-Mercapto-1-Propansulfonate and 1-Thioglucose Mixed Thiols for Antibacterial Applications. Materials (Basel). No. 12, 1028.

(7). Battocchio C, Meneghini C, Fratoddi I, Venditti I, Russo MV, Aquilanti G, Maurizio C, Bondino F, Matassa R, Rossi M, et al. (2012) Silver Nanoparticles Stabilized with Thiols: A Close Look at the Local Chemistry and Chemical Structure. J. Phys. Chem 116, 19571–19578.

(8). Stewart A, Zheng S, McCourt MR, and Bell SEJ (2012) Controlling Assembly of Mixed Thiol Monolayers on Silver Nanoparticles to Tune Their Surface Properties. ACS Nano 6, 3718–3726. [PubMed: 22500816]

(9). Trilling AK, Beekwilder J, and Zuilhof H (2013) Antibody Orientation on Biosensor Surfaces: A Minireview. Analyst 138, 1619–1627. [PubMed: 23337971]

(10). Basu Neogi P, Gryczynski Z, Choi TY, Neogi A, Calander N, Kim M, Lee KM, Luchowski R, and Kim B (2011) Silver Nanostructure Sensing Platform for Maximum-Contrast Fluorescence Cell Imaging. J. Biomed. Opt 16, 056008. [PubMed: 21639576]

(11). Goldman YE, Cooperman BS, Mandecki W, Smilansky Z, Kaur J, Chen C, Stevens B, Bharill S, Gryczynski Z, and Gryczynski I (2010) Enhancement of Single-Molecule Fluorescence Signals by Colloidal Silver Nanoparticles in Studies of Protein Translation. ACS Nano No. 1, 399–407. [PubMed: 21158483]

(12). Tripathi K, and Driskell JD (2018) Quantifying Bound and Active Antibodies Conjugated to Gold Nanoparticles: A Comprehensive and Robust Approach to Evaluate Immobilization Chemistry. ACS Omega 3, 8253–8259. [PubMed: 30087938]

(13). Wiseman ME, and Frank CW (2012) Antibody Adsorption and Orientation on Hydrophobic Surfaces. Langmuir 28, 1765–1774. [PubMed: 22181558]

(14). Bard AJ, and Faulkner LR (2001) Electrochemical Methods: Fundamentals and Applications (Harris D, Swain E, Robey C, Aiello E, Eds.) John Wiley & Sons, Inc, Hoboken.

(15). Ruiz G, Tripathi K, Okyem S, and Driskell JD (2019) PH Impacts the Orientation of Antibody Adsorbed onto Gold Nanoparticles. Bioconjugate Chem 30, 1182–1191.

(16). Karami P, Khoshsafar H, Johari-Ahar M, Arduini F, Afkhami A, and Bagheri H (2019) Colorimetric Immunosensor for Determination of Prostate Specific Antigen Using Surface Plasmon Resonance Band of Colloidal Triangular Shape Gold Nanoparticles. Spectrochim. Acta - Part A Mol. Biomol. Spectrosc 222, 117218.

(17). Hu T, Chen C, Huang G, and Yang X (2016) Antibody Modified-Silver Nanoparticles for Colorimetric Immuno Sensing of Aβ(1–40/1–42) Based on the Interaction between β-Amyloid and Cu2+. Sensors Actuators B Chem 234, 63–69.

(18). Rekha CR, Nayar VU, and Gopchandran KG (2018) Synthesis of Highly Stable Silver Nanorods and Their Application as SERS Substrates. J. Sci. Adv. Mater. Devices 3, 196–205.

(19). Oraevsky AA (2015) "Contrast Agents for Optoacoustic Imaging: Design and Biomedical Applications." Photoacoustics 3, 1–2. [PubMed: 25893168]

(20). Arruebo M, Valladares M, and González-Fernández Á (2009) Antibody-Conjugated Nanoparticles for Biomedical Applications. J. Nanomater 2009, 1–24.

(21). Cunningham JC, Scida K, Kogan MR, Wang B, Ellington AD, and Crooks RM (2015) Paper Diagnostic Device for Quantitative Electrochemical Detection of Ricin at Picomolar Levels. Lab Chip 15, 3707–3715. [PubMed: 26224395]

(22). Degregory PR, Tsai YJ, Scida K, Richards I, and Crooks RM (2016) Quantitative Electrochemical Metalloimmunoassay for TFF3 in Urine Using a Paper Analytical Device. Analyst 141, 1734–1744. [PubMed: 26824090]

(23). Scida K, Cunningham JC, Renault C, Richards I, and Crooks RM (2014) Simple, Sensitive, and Quantitative Electrochemical Detection Method for Paper Analytical Devices. Anal. Chem 86, 6501–6507. [PubMed: 24918259]

(24). DeGregory PR, Tapia J, Wong T, Villa J, Richards I, and Crooks RM (2017) Managing Heart Failure at Home With Point-of-Care Diagnostics. IEEE J. Transl. Eng. Heal. Med 1–6.

(25). Sokolov K, Follen M, Aaron J, Pavlova I, Malpica A, Lotan R, and Richards-Kortum R (2003) Real-Time Vital Optical Imaging of Precancer Using Anti-Epidermal Growth Factor Receptor Antibodies Conjugated to Gold Nanoparticles. Cancer Res 1999–2004. [PubMed: 12727808]

(26). Szymanski MS, and Porter RA (2013) Preparation and Quality Control of Silver Nanoparticle-Antibody Conjugate for Use in Electrochemical Immunoassays. J. Immunol. Methods 387, 262–269. [PubMed: 23153725]

(27). Buijs J, Lichtenbelt JWT, Norde W, and Lyklema J (1995) Adsorption of Monoclonal IgGs and Their F(Ab′)2 Fragments onto Polymeric Surfaces. Colloids Surfaces B Biointerfaces 5, 11–23.

(28). Siriwardana K, Wang A, Vangala K, Fitzkee N, and Zhang D (2013) Probing the Effects of Cysteine Residues on Protein Adsorption onto Gold Nanoparticles Using Wild-Type and Mutated GB3 Proteins. Langmuir 29, 10990–10996. [PubMed: 23927741]

(29). Ruiz G, Ryan N, Rutschke K, Awotunde O, and Driskell JD (2019) Antibodies Irreversibly Adsorb to Gold Nanoparticles and Resist Displacement by Common Blood Proteins. Langmuir 35, 10601–10609. [PubMed: 31335148]

(30). Weisbecker S, Merritt V, Weisbecker CS, Merritt MV, and Whitesidesx GM (1996) Molecular of Aliphatic Thiols on Gold Golloids. Langmuir 3763–3772.

(31). Canaria CA, Maloney JR, Yu CJ, Smith JO, Fraser SE, and Lansford R (2005) Formation of Biotinylated Alkylthiolate Self-Assembled Monolayers on Gold. Nanotechnology 321–324.

(32). Kogan MR, Pollok NE, and Crooks RM (2018) Detection of Silver Nanoparticles by Electrochemically Activated Galvanic Exchange. Langmuir 15719–15726. [PubMed: 30525650]

(33). Li X, Scida K, and Crooks RM (2015) Detection of Hepatitis B Virus DNA with a Paper Electrochemical Sensor. Anal. Chem 87, 9009–9015. [PubMed: 26258588]

(34). Cunningham JC, Kogan MR, Tsai Y-J, Luo L, Richards I, and Crooks RM (2016) Paper-Based Sensor for Electrochemical Detection of Silver Nanoparticle Labels by Galvanic Exchange. ACS Sensors 1, 40–47.

(35). Cheng X, Liu M, Zhang A, Hu S, Song C, Zhang G, and Guo X (2015) Size-Controlled Silver Nanoparticles Stabilized on Thiol-Functionalized MIL-53(Al) Frameworks. Nanoscale 7, 9738–9745. [PubMed: 25963664]

(36). Cunningham JC, Brenes NJ, and Crooks RM (2014) Paper Electrochemical Device for Detection of DNA and Thrombin by Target-Induced Conformational Switching. Anal. Chem 86, 6166–6170. [PubMed: 24871788]

(37). Huang T, Nallathamby PD, Gillet D, and Xu XHN (2007) Design and Synthesis of Single-Nanoparticle Optical Biosensors for Imaging and Characterization of Single Receptor Molecules on Single Living Cells. Anal. Chem 79, 7708–7718. [PubMed: 17867652]

(38). Guler Z, and Sarac AS (2016) Electrochemical Impedance and Spectroscopy Study of the EDC/NHS Activation of the Carboxyl Groups on Poly(ε-Caprolactone)/Poly(m-Anthranilic Acid) Nanofibers. Express Polym. Lett 10, 96–110.

(39). Kaghu RV, Sarma A, Silverton EW, and Terryi DD (1971) The Three-Dimensional Structure at 6 A Resolution Human Molecule. Biol. Chem 3753–3759.

(40). McCombs JR, and Owen SC (2015) Antibody Drug Conjugates: Design and Selection of Linker, Payload and Conjugation Chemistry. AAPS J 17, 339–351. [PubMed: 25604608]

(41). Treuel L, Brandholt S, Maffre P, Wiegele S, Shang L, and Nienhaus GU (2014) Impact of Protein Modification on the Protein Corona on Nanoparticles and Nanoparticle-Cell Interactions. ACS Nano 8, 503–513. [PubMed: 24377255]

(42). Grubisha DS, Lipert RJ, Park HY, Driskell J, and Porter MD (2003) Femtomolar Detection of Prostate-Specific Antigen: An Immunoassay Based on Surface-Enhanced Raman Scattering and Immunogold Labels. Anal. Chem 75, 5936–5943. [PubMed: 14588035]

(43). Lin PC, Chen SH, Wang KY, Chen ML, Adak AK, Hwu JRR, Chen YJ, and Lin CC (2009) Fabrication of Oriented Antibody-Conjugated Magnetic Nanoprobes and Their Immunoaffinity Application. Anal. Chem 81, 8774–8782. [PubMed: 19874051]

(44). Liddell E (2013) The Immunoassay Handbook: Theory and Applications of Ligand Binding, ELISA and Related Techniques (Wild DG, John R, Sheehan C, Binder S, He J, Eds.) Elsevier, Oxford.

(45). Chen YT, Medhi R, Nekrashevich I, Litvinov D, Xu S, and Lee TR (2018) Specific Detection of Proteins Using Exceptionally Responsive Magnetic Particles. Anal. Chem 90, 6749–6756. [PubMed: 29733644]

(46). Lin PC, Chen SH, Wang KY, Chen ML, Adak AK, Hwu JRR, Chen YJ, and Lin CC (2009) Fabrication of Oriented Antibody-Conjugated Magnetic Nanoprobes and Their Immunoaffinity Application. Anal. Chem 81, 8774–8782. [PubMed: 19874051]

(47). Wu X, Li Z, Chen XX, Fossey JS, James TD, and Jiang YB (2013) Selective Sensing of Saccharides Using Simple Boronic Acids and Their Aggregates. Chem. Soc. Rev 42, 8032–8048. [PubMed: 23860576]

(48). Haiss W, Thanh NTK, Aveyard J, and Fernig DG (2008) Determination of Size and Concentration of Gold Nanoparticles from Extinction Spectra. Anal. Chem 80, 6620–6625. [PubMed: 18642876]

(49). Rahme K, Chen L, Hobbs RG, Morris MA, O'Driscoll C, and Holmes JD (2013) PEGylated Gold Nanoparticles: Polymer Quantification as a Function of PEG Lengths and Nanoparticle Dimensions. RSC Adv 3, 6085–6094.

(50). Umadevi M (2017) Fluorescence Quenching by Plasmonic Silver Nanoparticles (Geddes CD, Ed.) pp 197–202, John Wiley & Sons, Inc.

(51). Kavitha SR, Umadevi M, Vanelle P, Terme T, and Khoumeri O (2014) Spectral Investigations on the Influence of Silver Nanoparticles on the Fluorescence Quenching of 1,4-Dimethoxy-2,3-Dibromomethylanthracene-9,10-Dione. Eur. Phys. J. D 68.

(52). Kavitha SR, Umadevi M, Vanelle P, Terme T, and Khoumeri O (2014) Spectral Investigations on the Fluorescence Quenching of 1,4-Dihydroxy-2,3-Dimethylanthracene-9,10-Dione by Plasmonic Silver Nanoparticles. Plasmonics 9, 443–450.

(53). Filbrun SL, and Driskell JD (2016) A Fluorescence-Based Method to Directly Quantify Antibodies Immobilized on Gold Nanoparticles. Analyst 141, 3851–3857. [PubMed: 27113720]

(54). Zhang L, Hu D, Salmain M, Liedberg B, and Boujday S (2019) Direct Quantification of Surface Coverage of Antibody in IgG-Gold Nanoparticles Conjugates. Talanta 204, 875–881. [PubMed: 31357376]

(55). Liu S, Horak J, Höldrich M, and Lämmerhofer M (2017) Accurate and Reliable Quantification of the Protein Surface Coverage on Protein-Functionalized Nanoparticles. Anal. Chim. Acta 989, 29–37. [PubMed: 28915940]

(56). Moulin AM, Shea SJO, and Welland ME (1999) Microcantilever-Based Biosensors. Ultramicroscopy No. 2000, 23–31. [PubMed: 10321038]

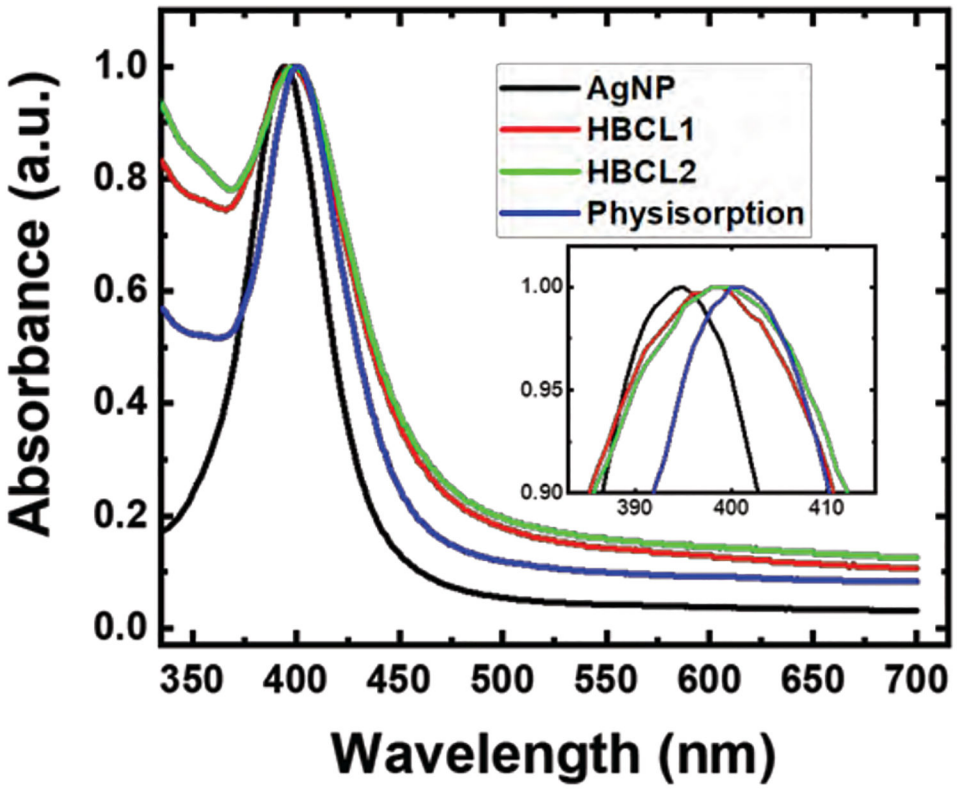

Figure 1.

Normalized UV-Vis spectra of the citrate-capped AgNPs (black) and the AgNPs after bioconjugation with Ab-HBCL1 (red), Ab-HBCL2 (green), and unmodified Abs (physisorption, blue). The inset is an expanded view of the maxima of the plasmon peaks: λ_{max} = 395, 398, 398, and 400 nm for citrate-capped AgNPs, AgNP-HBCL1-Ab, AgNP-HBCL2-Ab, and physisorbed conjugates, respectively. The spectra are representative of three independent measurements, and λ_{max} did not shift within precision of the measurement (accuracy within 1 nm) for the three trials.

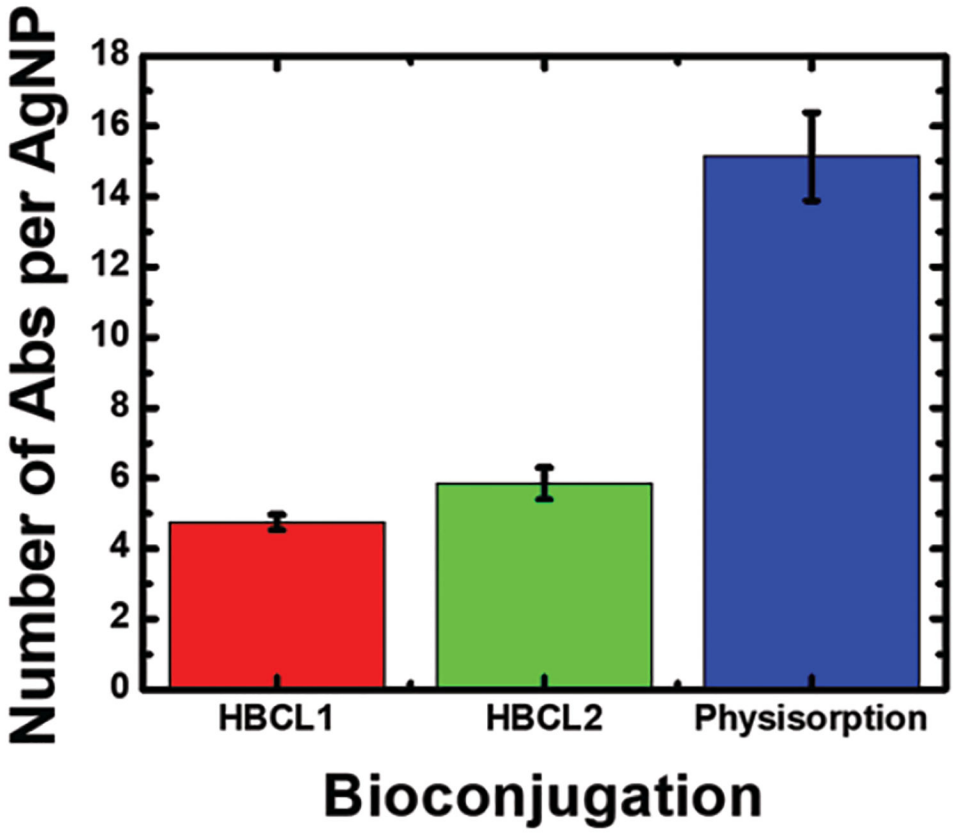

Figure 2.

Histogram showing the number of Abs bound per AgNP for each of the conjugation methods. The data were obtained using an indirect enzyme-linked immunosorbent assay (ELISA). The error bars represent the standard deviation of three independent measurements. Additional information about the measurement is provided in Figure S2.

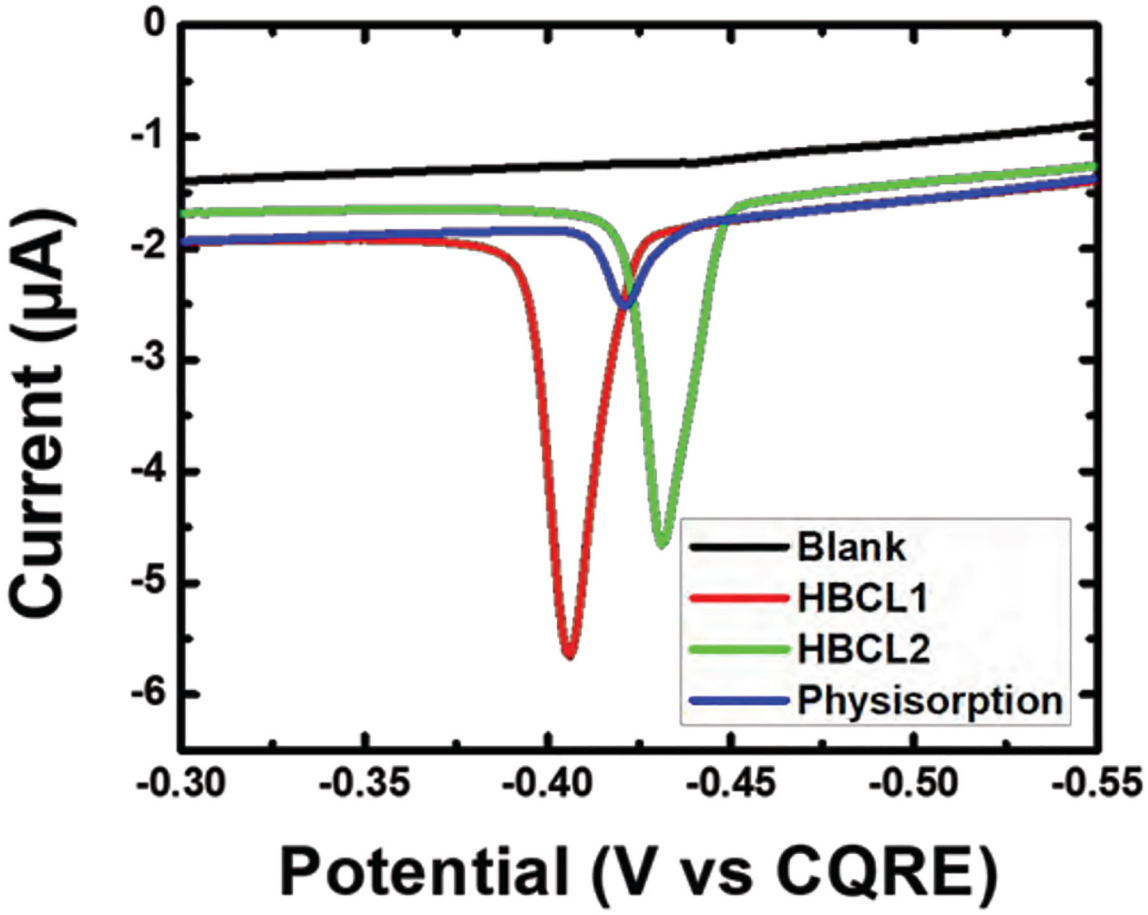

Figure 3.

Anodic stripping voltammograms (ASVs) obtained by forming a half-metalloimmunoassay with the conjugates in a microtiter plate, adding $KMnO_4$ to oxidize bound AgNPs, transferring the entire contents of each well to a carbon paste working electrode, and then carrying out the electrochemical protocol discussed in the text. The scan rate was 50 mV/s. For clarity, only one ASV trace is shown for each conjugate, but the measurements were carried out in triplicate. The position of the ASV peaks varies due to the use of a quasi-carbon reference electrode.

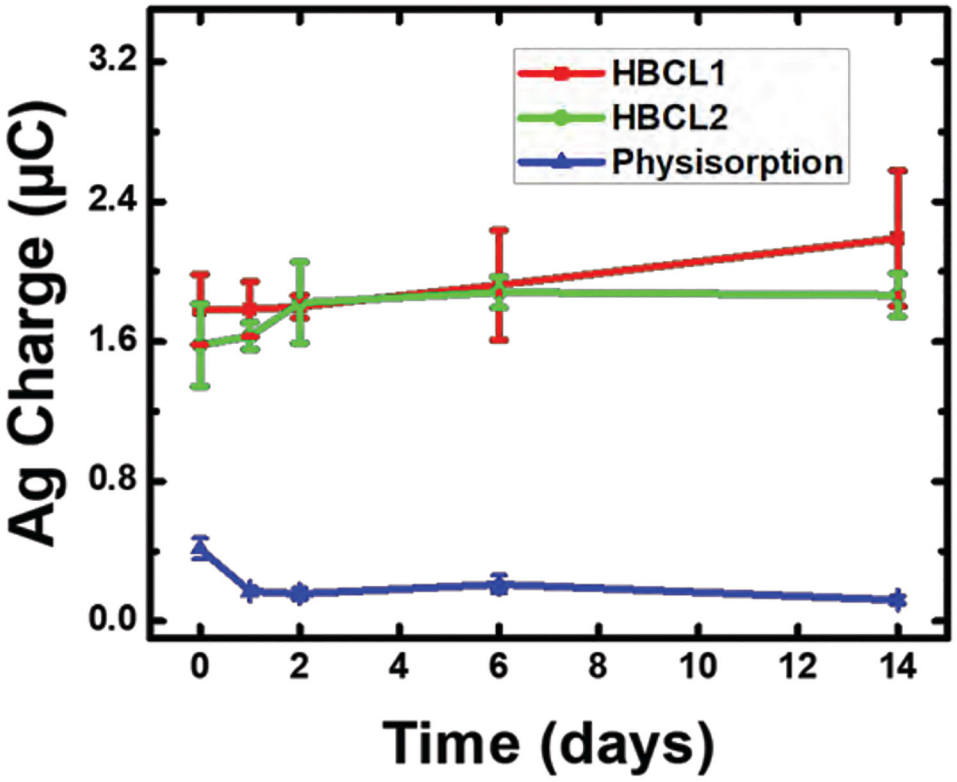

Figure 4.

Ag charge obtained for the conjugates using the same electrochemical protocol as in Figure 3, but performed on days 0, 1, 2, 6, and 14. Day 0 indicates the day the conjugates were prepared. Each data point represents the standard deviation from the mean for three replicate measurements obtained using independently prepared electrodes.

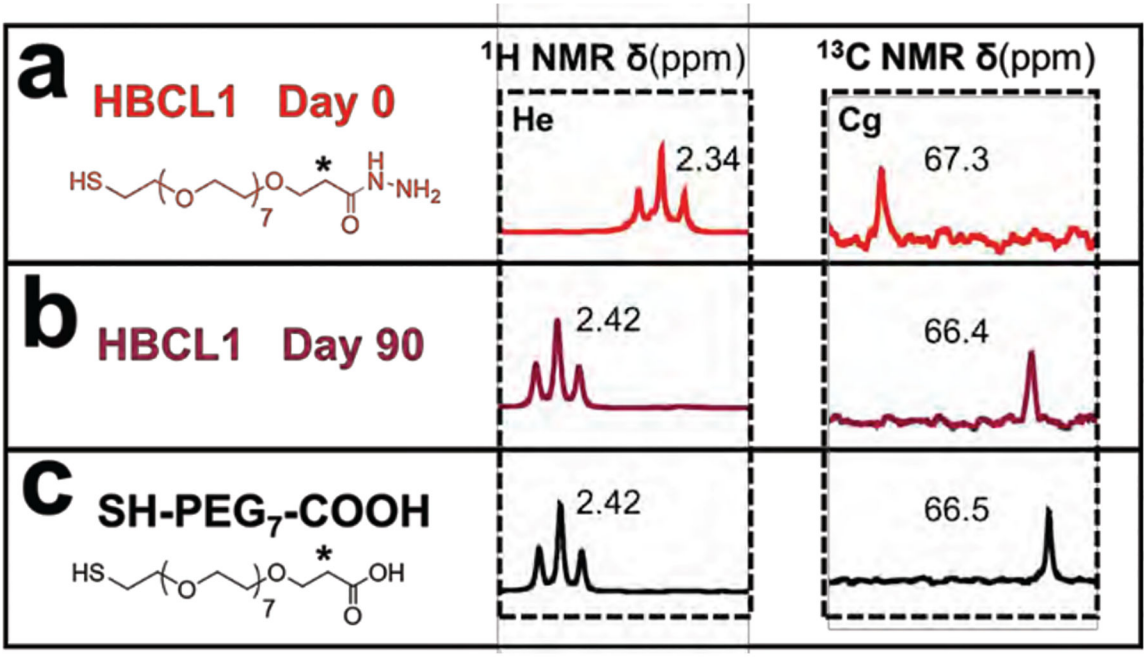

Figure 5.

Stability study of HBCL1 (just the linker, not the full conjugate) as a function of time. The ^{1}H and ^{13}C NMR (400 MHz, $DMSO_{d6}$) spectra of HBCL1 are shown at (a) day 0 and (b) day 90. The cross-linker was stored in DI water during the 90-day period. **He** and **Cg** peaks are denoted by an asterisk. Figure S5 provides complete labeling of the spectra. (c) The ^{1}H and ^{13}C NMR (400 MHz, $DMSO_{d6}$) spectra of SH-PEG_7-COOH.

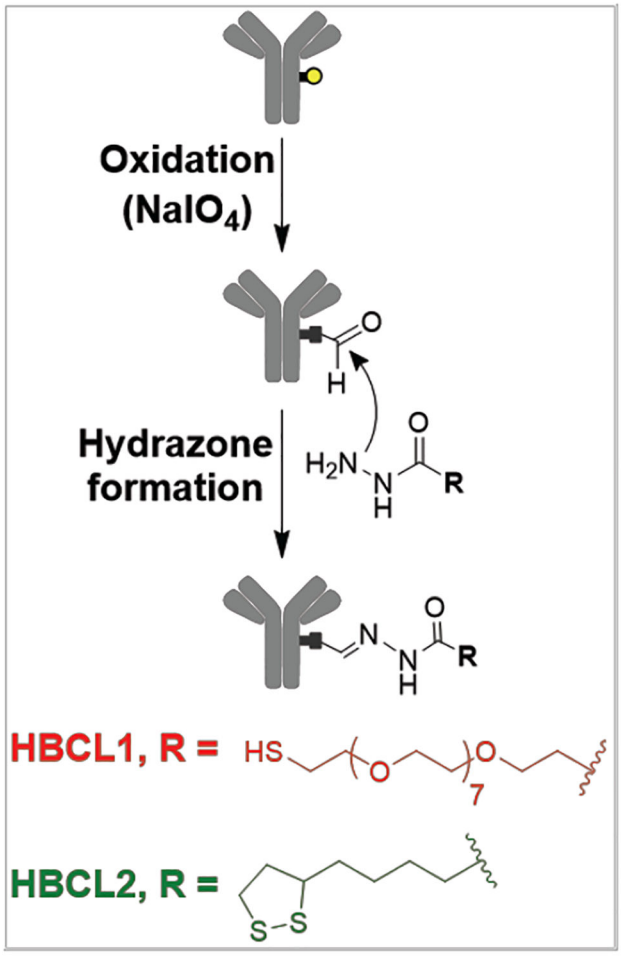

Scheme 1.